

Uncertainty Quantification for Prior-Data Fitted Networks using Martingale Posteriors

Thomas Nagler

Department of Statistics, LMU Munich
Munich Center for Machine Learning

David Rügamer

Abstract

Prior-data fitted networks (PFNs) have emerged as promising foundation models for prediction from tabular datasets, achieving state-of-the-art performance on small to moderate data sizes without tuning. While PFNs are motivated by Bayesian ideas, they do not provide any uncertainty quantification for predictive means, quantiles, or similar quantities. We propose a principled and efficient sampling procedure to construct Bayesian posteriors for such estimates based on martingale posteriors, and prove its convergence. Several simulated and real-world data examples showcase the uncertainty quantification of our method in inference applications.

1 INTRODUCTION

Prior-data fitted networks (PFNs) are foundation models (Hollmann et al., 2023; Müller et al., 2022) that allow for in-context learning, i.e., the ability to learn at inference time without any parameter updates (Garg et al., 2022). TabPFN, a transformer pre-trained on synthetic data for in-context learning on tabular datasets, has recently attracted a lot of interest. TabPFN (Hollmann et al., 2023, 2025) and extensions such as TuneTables (Feuer et al., 2024) and LocalPFN (Thomas et al., 2024) have been shown to achieve state-of-the-art performance on tabular benchmarks by pre-training on purely synthetic data. Since PFNs and extensions learn in-context, there is no need for further model (fine-)tuning on the inference task.

Recent extensions of PFNs allow their applicability to large datasets (Feuer et al., 2024), the use of PFN “priors” for latent variable models (Reuter et al., 2025), and simultaneously minimizing bias and variance to improve their performance (Liu and Ye, 2025). PFNs are also related to simulation-based inference and amortized inference but have slightly different goals and

do not amortize across a single but multiple datasets (Reuter et al., 2025). While introduced as a Bayesian method and approximation to the posterior predictive, PFNs can also be interpreted as pre-tuned untrained predictors (Nagler, 2023). This also relates to the question of what uncertainty PFN models can provide.

PFNs approximate the posterior predictive distribution for the label given some feature values. Despite the name, this only yields point estimates of the most relevant predictive quantities, such as the conditional mean or quantiles. Due to the complex nature of PFNs, it is difficult to assess the uncertainty of these point estimates.

We propose a principled and efficient method to construct Bayesian posteriors for such estimates using the idea of *Martingale Posteriors* (MPs). In particular:

1. We introduce a new extension of the MP framework of Fong et al. (2023) for inference of predictive quantities conditional on a specific feature value x .
2. We propose an efficient, nonparametric resampling scheme yielding an approximate posterior for the point estimates derived from a PFN, and prove its convergence.
3. We extend existing learning rate schedules and discuss the role of contraction rates in light of inconsistent PFN estimators.
4. We illustrate the new method in several simulated and real-world data applications.

Our work provides an essential tool for principled inference with the exponentially popular PFN methods. A brief discussion of potential extensions to large language models is provided in Section 5.

2 BACKGROUND

We consider a tabular prediction task with labels $y \in \mathbb{R}$ and features $x \in \mathbb{R}^d$ drawn from a joint distribution P .

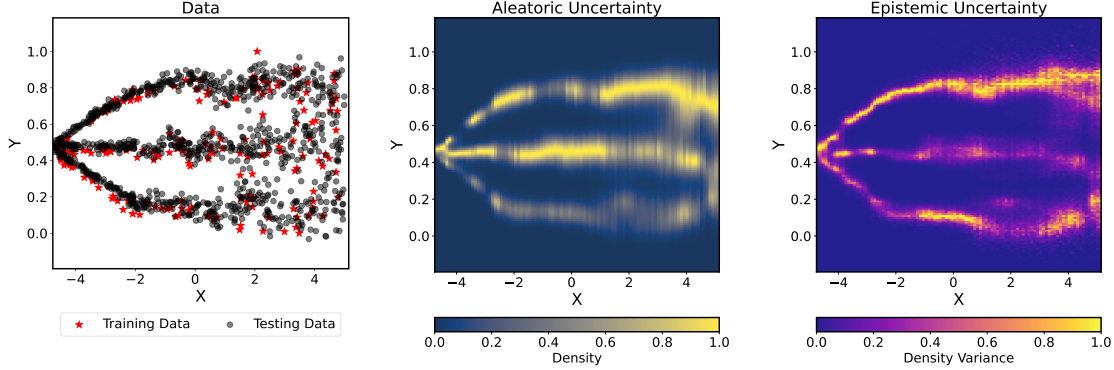


Figure 1: Visualization of the diffusion process data (left) together with the PFN predicted density (center) and the estimated epistemic uncertainty (right) via our martingale posterior approach.

A typical problem in such tasks is to estimate predictive quantities such as conditional means $\mathbb{E}[y|x]$, conditional probabilities $P(y|x)$, or conditional quantiles $P^{-1}(\alpha|x)$. Because the true distribution P is unknown and only a finite amount of data $\mathcal{D}_n = (y_i, x_i)_{i=1}^n$ is available, estimates of such quantities bear some uncertainty. Our goal is to quantify this uncertainty.

2.1 Prior-Data Fitted Networks

Prior-data fitted networks are foundation models trained to approximate the posterior predictive density

$$\text{PPD}(y|x) = p(y|x, \mathcal{D}_n),$$

which quantifies the likelihood of observing label y given that the feature is x and \mathcal{D}_n has been observed. The PPD is a Bayesian concept and implicitly involves a prior over the distributions P that could have generated the data. To approximate the PPD with a PFN, a deep neural network—typically a transformer—is pre-trained on simulated datasets with diverse characteristics. After pre-training, the network weights are fixed, and the approximate PPD for a new training set can be computed through a single forward pass without additional training or tuning. The PPD quantifies uncertainty about the label y . However, it mixes the aleatoric and epistemic components of uncertainty (Hüllermeier and Waegeman, 2021). From the PPD alone, it is impossible to disentangle these parts. Consequently, PFNs do *not* provide uncertainty estimates for predictive summaries, such as conditional mean, probabilities, and quantiles (see Figure 1).

2.2 Bayesian Inference

In classical Bayesian inference, the set of possible distributions $P = P_\theta$ is indexed by some parameter θ . A *prior* distribution $\pi(\theta)$ is elicited to quantify our beliefs about the likelihood of the possible values of θ

before seeing any data. After observing \mathcal{D}_n , this belief is updated to a *posterior* $\pi(\theta|\mathcal{D}_n)$ of the parameter θ given the data. For predictive inference, the PPD can be computed as

$$\text{PPD}(y|x) = \int p_\theta(y|x) \pi(\theta|\mathcal{D}_n) d\theta.$$

In contrast to the PPD, the posterior $\pi(\theta|\mathcal{D}_n)$ also quantifies uncertainty for other interest quantities. For example, the posterior distribution for the conditional mean $\mu(x) = \int y p_\theta(y|x) dy$ is given by

$$\Pi(\mu(x) \in A) = \int \mathbf{1} \left\{ \int y p_\theta(y|x) dy \in A \right\} \pi(\theta|\mathcal{D}_n) d\theta,$$

for any $A \subseteq \mathbb{R}$. PFNs neither provide an explicit model for p_θ nor an explicit prior $\pi(\theta)$, although both may be implicit in the PPD. The following shows how Bayesian posterior inference can be approached when only the PPD is available.

2.3 Martingale Posteriors

Martingale posteriors were recently introduced by Fong et al. (2023) as a new method for Bayesian uncertainty quantification. Its core idea is to reverse the direction of the Bayesian inference. In classical Bayesian inference, the posterior is derived from a prior and likelihood, which then implicitly leads to the PPD. MP inference starts from the PPD and leaves the prior $\pi(\theta)$ implicit. An appropriate sampling scheme and Doob's theorem then allow us to derive posteriors for virtually all quantities of interest (e.g., the conditional mean $\mu(x)$).

To simplify our outline of the approach, consider the case where there are no features, and we are interested in unconditional inference. An extension to our predictive inference setting will be made explicit in Section 3.1. Suppose we have observed data $y_{1:n} = (y_1, \dots, y_n)$.

The MP approach involves iteratively sampling

$$y_{n+1} \sim p(\cdot | y_{1:n}), \quad y_{n+2} \sim p(\cdot | y_{1:(n+1)}), \quad (1)$$

$$y_{n+3} \sim p(\cdot | y_{1:(n+2)}), \quad \dots \quad (2)$$

N times, which yields a sample $y_{(n+1):(n+N)}$ drawn from the predictive joint distribution

$$p(y_{(n+1):(n+N)} | y_{1:n}) = \prod_{i=1}^N p(y_{n+i} | y_{1:(n+i-1)}).$$

Observe, however, that the samples are neither independent nor identically distributed. As a consequence, the long-run empirical distribution of the obtained sample,

$$F_\infty(y) = \lim_{N \rightarrow \infty} \frac{1}{N} \sum_{i=1}^N \mathbf{1}(y_{n+i} \leq y),$$

is a random function and comes out differently whenever the sampling procedure is repeated. Denote by $\Pi(F_\infty | \mathcal{D}_n)$ the distribution of this function (which depends on the data \mathcal{D}_n we start with). For any parameter $\theta = \theta(P)$ of interest, the martingale posterior is now given as

$$\Pi(\theta \in A | \mathcal{D}_n) = \int \mathbf{1}\{\theta(F_\infty) \in A\} d\Pi(F_\infty | \mathcal{D}_n),$$

where A is any Borel set on the space where the parameter θ lives. Furthermore, Doob's theorem (Doob, 1949) implies that $\Pi(\theta | \mathcal{D}_n)$ coincides with the classical Bayes posterior for the prior $\pi(\theta)$ implicit in the PPD (Fong et al., 2023).

3 EFFICIENT MARTINGALE POSTERIORS FOR PRIOR-DATA FITTED NETWORKS

Martingale posteriors allow for Bayesian inference directly from the PPD. PFNs approximate the PPD, so using PFNs to construct a martingale posterior seems natural. However, there are two problems. First, modern PFNs are based on transformer architectures that require $\Omega(n^2)$ operations for a forward pass on a training set size of n . Iteratively computing $p(y | y_{1:(n+k)})$ for $k = 1, \dots, N$ thus has complexity $\Omega(N^3)$, which is prohibitive. Second, Falck et al. (2024) found that modern transformer-based LLMs substantially deviate from the *martingale property*

$$\mathbb{E}[p(y | y_{1:(n+k)}) | y_{1:n}] = p(y | y_{1:n}).$$

Also TabPFN fails in this regard.

Figure 2 (experiment description in Section 4.1) shows a QQ-plot of the average CDF resulting from PFN's PPD at iteration 0 vs. the CDF after k forward iterations

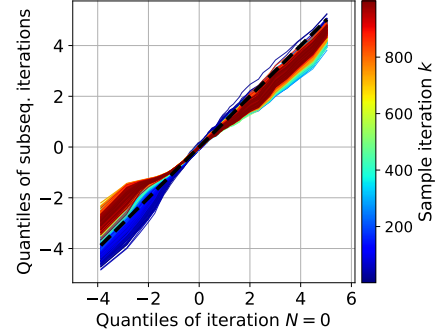


Figure 2: PFN's initial CDF (x-axis) vs. its average CDF of subsequent iterations (y-axis).

of the sampling procedure. The martingale property is satisfied when this distribution remains constant, i.e., all lines lie on the $x = y$ diagonal. However, we see an apparent change in the distribution over the different sampling horizons. This reinforces that PFNs approximate Bayesian inference only in a weak sense, even though they were conceived from Bayesian ideas (Hollmann et al., 2023; Müller et al., 2021).

Without the martingale property, the MP sampling procedure leads to meaningless results. Instead, we propose to use the PPD implied by the PFN only as a starting point for the sampling scheme. This PPD is then iteratively updated using the nonparametric Gaussian copula approach of Fong et al. (2023), which ensures the martingale property. The resulting martingale posterior effectively treats the PFN output as an informed prior, without requiring the PFN to provide coherent posterior updates.

3.1 Martingale Posteriors for Conditional Inference

We extend the unconditional sampling scheme outlined in the previous section to the conditional inference setting. Fong et al. (2023) already proposed one such extension. Their scheme involves forward sampling of the features $x_{(n+1):(n+N)}$. The distribution of the features isn't of primary interest but significantly complicates the sampling procedure, which the authors resolved through heuristic simplifications. In contrast to Fong et al. (2023), we propose to sample only the labels $y_{(n+1):(n+N)}$ conditional on the event that $x_{n+k} = x$, for a fixed value of x and all $k = 1, \dots, N$.

Specifically, our goal is to simulate data from the distribution

$$p(y_{(n+1):(n+N)} | x_{(n+1):(n+N)} = x, \mathcal{D}_n).$$

Set $x_{n+k} = x$ for all $k \geq 1$, and define

$$p_k(y) = p(y_{n+k+1} | y_{1:(n+k)}, x_{1:(n+k)}),$$

and P_k as the corresponding CDF. Applying Bayes' rule recursively gives

$$p(y_{(n+1):(n+N)}|x_{(n+1):(n+N)} = x, \mathcal{D}_n) = \prod_{k=n}^{N-1} p_k(y_{k+1}),$$

which suggests that we can iteratively sample

$$y_{n+1} \sim P_0, \quad y_{n+2} \sim P_1, \quad y_{n+3} \sim P_2, \quad \dots$$

Denote the long-run empirical distribution of the obtained sample by

$$F_{\infty,x} = \lim_{N \rightarrow \infty} \frac{1}{N} \sum_{i=1}^N \mathbb{1}(y_{n+i} \leq y),$$

which is again a random function, even in the limit. Repeating the iterative sampling procedure gives us its distribution $\Pi(F_{\infty,x}|\mathcal{D}_n)$. For any conditional parameter $\theta(x) = \theta(P(\cdot|x))$ of interest, the martingale posterior is now given as

$$\Pi(\theta(x) \in A|\mathcal{D}_n) = \int \mathbb{1}\{\theta(F_{\infty,x})\} d\Pi(F_{\infty,x}|\mathcal{D}_n).$$

Common examples of the parameter $\theta(x)$ are the conditional mean $\theta(x) = \int y dP(y|x) dy$ or a conditional ϱ -quantile $\theta(x) = P^{-1}(\varrho|x)$.

3.2 Efficient PPD Updates Based on the Gaussian Copula

Observe that $p_0(y) = p(y|x, \mathcal{D}_n)$ is the PPD approximated by the PFN g_θ . However, the following update distributions p_1, p_2, \dots are generally intractable. To alleviate this, Fong et al. (2023) proposed a computationally efficient, nonparametric method based on Dirichlet Process Mixture Models (DPMMs) and a copula decomposition of the conditional p_k . Specifically, we set

$$\begin{aligned} P_k(y) = & (1 - \alpha_{n+k}) P_{k-1}(y) \\ & + \alpha_{n+k} H_\rho(P_{k-1}(y), P_{k-1}(y_{n+k})), \end{aligned} \quad (3)$$

where P_k is the CDF corresponding to p_k , $\alpha_i = (2 - i^{-1})(i + 1)^{-1}$,

$$H_\rho(u, v) = \Phi \left(\frac{\Phi^{-1}(u) - \rho \Phi^{-1}(v)}{\sqrt{1 - \rho^2}} \right),$$

and Φ is the standard normal cumulative distribution function. The method has a hyperparameter ρ , corresponding to a bandwidth that smoothes the updates. Fong et al. (2023) proposed to tune this by maximizing the likelihood of the updated densities over the observed data. To increase the alignment of the updates with the PFN baseline, we simulate a new sample from the PFN and optimize the bandwidth on the simulated data. More details can be found in Section B.1

3.3 Flexible Learning Rate Schedules

Fong et al. (2023) suggested the learning rate $\alpha_i = (2 - i^{-1})(i + 1)^{-1}$ for the unconditional context, where distribution functions can be estimated with convergence rate $n^{-1/2}$. As we shall see in Proposition 3 below, the learning rate α_i determines the contraction rate of the posterior. Our setting, however, is conditional on $x \in \mathbb{R}^d$, where nonparametric methods such as TabPFN must converge slower than $n^{-1/2}$, with rates depending on the dimension and smoothness of the estimation problem (see, e.g., Stone, 1982).

To accommodate such settings, we allow for more flexible learning rate schedules that can be calibrated to match the behavior of the PFN. Specifically, we parametrize the learning rate as

$$\alpha_{n+k} = C(n + k + 1)^{-\beta}, \quad C \in (0, \infty), \beta \in (0, 1].$$

where C and β should be chosen such that the behavior of the update (3) roughly matches the behavior of the PFN. In our experiments, we implement the following three schedules

- default: $C = 2, \beta = 1$ as in (Fong et al., 2023),
- type 1: $C = 10^{-(d-1)/(d+4)}, \beta = 1/2 + d/(d+4)$,
- type 2: $C = 10^{-2d/(d+4)}, \beta = d/(d+4)$.

The constants C are set to normalize the schedules to a comparable starting scales. We refer to our discussion after Proposition 3 in the next section for a motivation of the exponent β , and to Section 4.4 for empirical evaluation.

3.4 Theoretical Properties

Despite the simplicity of the updates given in (3), they provide essential theoretical guarantees. The following is a direct consequence of Theorem 3 by Fong et al. (2023).

Proposition 1. *It holds $(y_{N+1}, y_{N+2}, \dots) \rightarrow_d (z_1, z_2, \dots)$ as $N \rightarrow \infty$ where (z_1, z_2, \dots) has an exchangeable distribution.*

By de Finetti's theorem (e.g., Theorem 1.49 in Schervish, 2012), it then follows that there is a random variable Θ such that (z_1, z_2, \dots) is conditionally *iid* given Θ . The distribution of Θ can be interpreted as an implicit prior. In our setting, this prior depends both on the initial PPD implied by the PFN and the Gaussian copula updates specified by (3). In particular, the following result follows from Proposition 1 above and Theorem 2.2 of Berti et al. (2004).

Proposition 2. Suppose that P_0 is absolutely continuous with respect to the Lebesgue measure. Then there exists a random probability distribution $P_{\infty,x}$ such that $\lim_{N \rightarrow \infty} P_N(y) = P_{\infty,x}(y) = F_{\infty,x}(y)$ almost surely.

The proposition implies that the (random) limit $P_{\infty,x}$ is well defined and that the iterative sampling scheme is a valid way to draw from its distribution. We can be more precise about how fast this limit is approached.

Proposition 3. For any $y \in \mathbb{R}$, $N \geq 0$, the following holds with probability at least $1 - \delta$:

$$|P_{\infty,x}(y) - P_N(y)| \leq C \sqrt{\frac{\log(2/\delta)}{2\beta - 1}} (n + N)^{-\beta + 1/2}.$$

The proof, given in Section A, is based on a time-uniform version of the Azuma-Hoeffding concentration inequality (Howard et al., 2020), the martingale property of the copula updates, and the learning rate schedule. Importantly, time-uniform martingale concentration allows us to directly bound the deviation of interest $|P_{\infty,x} - P_N|$ as opposed to $|P_M - P_N|$ with $M \geq N$ as in Fong et al. (2023).

Proposition 3 quantifies how well the distribution P_N approximates $P_{\infty,x}$ after N updates. Setting $N = 0$ corresponds to the case where P_N equals the initial PPD given only the observed data. In our setting, this is the output from the PFN. The random limit $P_{\infty,x}$ fluctuates around this point estimate, and the spread of these fluctuations characterizes the spread of the martingale posterior for $\theta(P(\cdot|x))$.

3.5 The Role of β

The case $\beta = 1$ corresponds to the choice $\alpha_i \sim i^{-1}$ proposed by Fong et al. (2023) in the unconditional context with contraction rate of $n^{-1/2}$. Contraction rates for nonparametric regression problems are typically much slower than $n^{-1/2}$ (Ghosal and Van der Vaart, 2017, Chapter 9), however. To accommodate such slow contraction rates, it is therefore crucial to allow for learning rates with $\beta < 1$. The choice $\beta = d/(d+4)$ of our type 1 schedule corresponds to the optimal contraction rate we can expect in a nonparametric regression problem with d features and twice continuously differentiable regression curve. However, Nagler (2023) demonstrated that current PFN architectures yield inconsistent estimators, as their bias does not vanish as $n \rightarrow \infty$. This suggests that to get valid inferences, the posterior should never contract fully. This happens in the regime $\beta \in (0, 1/2]$, where the bound in Proposition 3 becomes vacuous, but the algorithm still converges to a random limit $P_{\infty,x}$ because of Proposition 2. This motivates the choice $\beta = 4/(d+4)$, which has $\beta \leq 1/2$ for the

regime $d \geq 4$, where the bias becomes notable already on moderate sample sizes.

3.6 Computation

In practice, we can only sample finite sequences and replace the MP by its finite approximation. The procedure is summarized in Algorithm 1. The overall run-time complexity of the algorithm is $O(BN)$, where B is the number of replications, and N is the length of one ‘chain’. Based on the considerations in the previous subsection, we recommend generating around $N = 200$ forward samples in each replication. The computations are independent across the outer loop iterations ($b = 1, \dots, B$) and straightforward to parallelize; the inner loop ($k = 1, \dots, N$) must be run sequentially. Except for the initial computation of $\widehat{\text{PPD}}(y|x)$, the runtime is independent of the dataset size n .

Algorithm 1 Computation of Martingale Posterior

```

1: Input: Estimated  $\widehat{\text{PPD}}(y|x)$  obtained from the
   PFN.
2: for  $b = 1, \dots, B$  do
3:   Initialize  $P_0^{(b)} \leftarrow \widehat{\text{PPD}}(y|x)$ .
4:   for  $k = 1, \dots, N$  do
5:     Sample  $y_{n+k}^{(b)} \sim P_{k-1}^{(b)}$ .
6:     Update  $(P_{k-1}^{(b)}, y_{n+k}^{(b)}) \rightarrow P_k^{(b)}$  as in (3).
7:   end for
8:   Compute  $\widehat{P}_N^{(b)}(y) = \frac{1}{N} \sum_{i=1}^N \mathbf{1}\{y_{n+i}^{(b)} \leq y\}$ .
9:   Set  $\theta^{(b)}(x) \leftarrow \theta(\widehat{P}_N^{(b)})$ .
10:  end for
11:  Compute the estimated Martingale Posterior:
     $\widehat{\Pi}(\theta(x) \in A | \mathcal{D}_n) = \frac{1}{B} \sum_{b=1}^B \mathbf{1}\{\theta^{(b)}(x) \in A\}.$ 

```

4 NUMERICAL EXPERIMENTS

To demonstrate the efficacy of our approach, we conduct various experiments. Here, we focus on conditional posterior and coverage properties, but we also provide further ablation studies to better understand our method’s behaviour. We use the aforementioned combination of DPMMs and copula decomposition in all cases. To estimate ρ , we always randomly draw 1000 data points simulated by the PFN. We use the original learning rate approach in the first three sections, but perform dedicated ablations for benchmarks. To this end, we will refer to our method with the learning rate proposed in Fong et al. (2023) as **Ours (default)**, while the adaptations proposed in Section 3.3 based on theoretical considerations and following the discussion about the biasedness of TabPFN are called **Ours (type 1)** and **Ours (type 2)**.

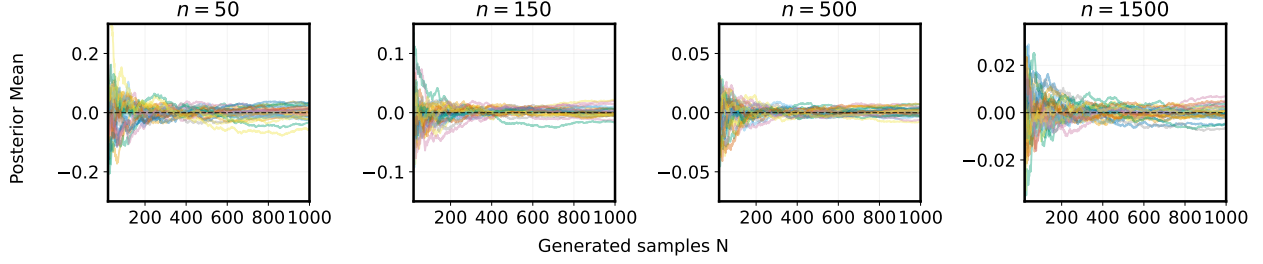


Figure 3: Effect of N on the convergence of P_N , depicted by $B = 30$ different PPD mean estimates.

4.1 TabPFN Martingale Property Check

In order to investigate whether TabPFN possesses the martingale property, we fit TabPFN using $n = 25$ data points of a Gamma distribution with scale and shape parameter 2. Following the martingale routine in (1), we then predict y_{n+k} for $k \in [1, 1000]$ and always add the previous iteration’s sample to the dataset to refit TabPFN. In each step, we compute TabPFN’s PPD.

Results As demonstrated in Figure 2, the resulting CDF of the iteratively updated PPD changes notably over time by first providing a wider PPD (all points of the QQ-plot lie below the bisecting line) and then becoming notably positively skewed for later iterations.

4.2 Convergence Speed

We start by investigating the convergence speed of the MP sampling algorithm. For this, we subsample the `concrete` dataset (Yeh, 1998) to generate datasets of different sizes. After standardizing the $n \in \{25, 100, 250, 1000\}$ data points, we visually inspect how the conditional posterior mean distribution of y_{n+k} conditional on fixed features x for $B = 30$ instances evolves when running our MP approach for $k \in (0, 1000]$ steps. Figure 3 summarizes the results for the default type learning rate and confirms that the different trajectories stabilize within the given budget of $N = 1000$ sampling steps independent of n . This is confirmed in all of our practical applications, where convergence is observed no later than after $N = 500$ steps. Results for different learning rate schedules are given in Section B.2.3.

4.3 Conditional Regression Posterior

Our approach enables posterior estimation given new features x , complementing PFN’s aleatoric uncertainty with epistemic uncertainty. We demonstrate this using a diffusion process ($n = 200$). This data is challenging as it evolves from an unimodal to a trimodal heteroscedastic Gaussian distribution with linear trends and sinusoidal changes depending on x . We run our

routine and compute both the estimated density by TabPFN and the variance of this density as a measure of epistemic uncertainty provided by our method.

Results The results are depicted in Figure 1. While TabPFN is able to fit the data-generating process well and its uncertainty (normalized density values) aligns with the apparent data for larger x values, higher density values also coincide with higher uncertainty (as measured by the normalized density variance). This becomes particularly visible in the lower branch of the diffusion process, where less training data is available. The provided density by TabPFN is comparatively small in this area, while the corresponding epistemic uncertainty is relatively large.

4.4 Benchmark

As an empirical evaluation, we compare our method using the previously presented learning rate approaches on real-world data from the UCI repository (Dua and Graff, 2017). We further compare against a bootstrap approach, which represents the natural comparison method, as it can also determine uncertainty for estimated parameters from PFN without additional parametric assumptions. In this benchmark, we run a conditional quantile regression ($\alpha \in \{0.5, 0.9\}$) on the datasets `airfoil` ($n = 1503$, $p = 5$), `boston` ($n = 252$, $p = 15$), `concrete` ($n = 1030$, $p = 8$, Yeh, 1998), `diabetes` ($n = 442$, $p = 10$, Efron et al., 2004), `energy` ($n = 768$, $p = 8$, Tsanas and Xifara, 2012), and `fish` ($n = 908$, $p = 6$). These datasets provide an ideal benchmark for PFNs, which are still limited in their scalability to larger datasets. We use $n = 100$ data points for training and aim to measure the uncertainty of PFN for the predicted quantile on the remaining data points. In addition to our approaches using the martingale posterior with $B = 100$, the non-parametric bootstrap is computed. The bootstrap reruns the PFN method for $R = 20$ times by drawing samples from the training dataset with replacement, makes quantile predictions, and computes the empirical 90% confidence interval of these predictions. We use both methods to construct a 90% credible/confidence interval (CI)

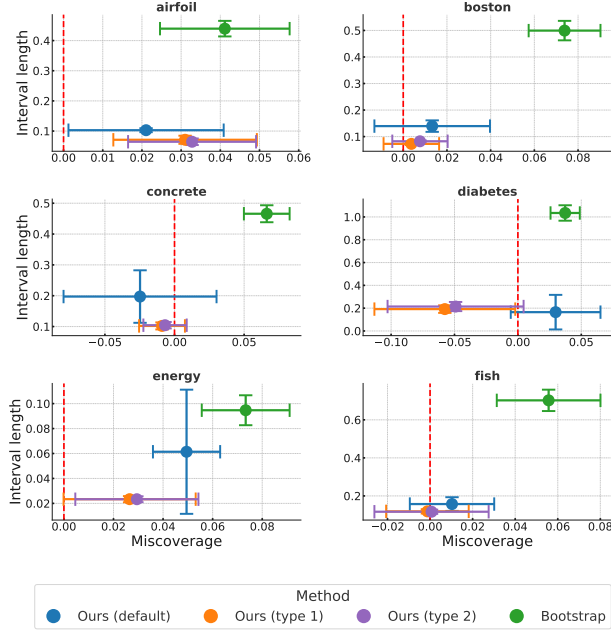


Figure 4: Mean values and standard deviations (error bars) of miscoverage (observed minus nominal value; x-axis) and interval length (y-axis) of the 90% credible intervals produced by the original method (blue), our proposed adaptations (orange, purple), and the bootstrap, across the different benchmark datasets. The red vertical line indicates perfect coverage.

and check the coverage of the predicted quantile given test dataset features. We also compute the length of these intervals to see how conservative our method is in comparison to a bootstrap approach, as well as the time for computation. We repeat the process five times with different splits.

Results Figure 4 summarizes the results of our benchmark for $\alpha = 0.5$, i.e., conditional median regression. The results are similar to those with smaller dataset size and for the quantile regression case (provided in Tables 3 and 4 in Section B), with our approach taking a fraction of the bootstrap approach’s time while yielding notably smaller CIs with better coverage. When comparing the different learning rate schemes, we see that in most cases, it is possible to either decrease the interval width (airfoil, boston, concrete, energy, fish) or improve the coverage (boston, concrete, energy, fish), or both, over the approach proposed in Fong et al. (2023).

Runtime In addition, Section B.2.5 provides a comparison that fixes the time budget of both the MP and the bootstrap approach. As the bootstrap takes notably longer than our method (requiring R forward passes of the PFN while our routine only uses PFNs once for P_0 and the estimation of ρ), the undercoverage

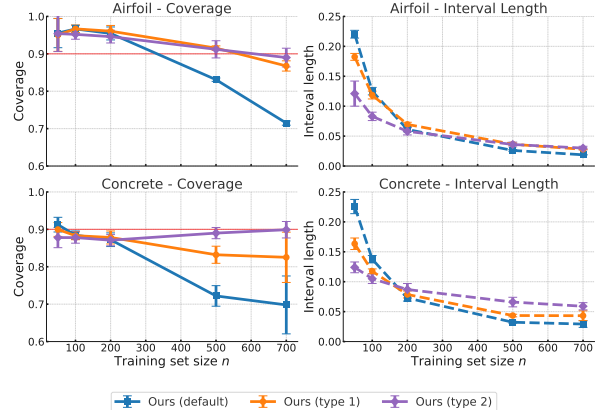


Figure 5: Coverage and interval length behavior for the larger UCI datasets (rows) for differently sized training datasets.

of the bootstrap becomes even more pronounced.

4.5 Ablation: Dataset Size

In the previous sections, the sizes of the datasets are relatively small. Using small datasets is done intentionally, as PFNs particularly shine in small-scale applications by leveraging their pretraining. Here, we further investigate how coverages change when increasing the dataset size using the two largest datasets (airfoil, concrete) from Section 4.4 and subsample the datasets to training data sizes of $n \in \{50, 100, 200, 500, 700\}$.

Failure due to Bias This analysis is particularly interesting in light of our discussion in Section 3.5, suggesting that intervals will not yield nominal coverage, even for $n \rightarrow \infty$ due to the non-vanishing bias of TabPFN. Empirically, this is validated in Figure 5, showing that neither the learning rate from Fong et al. (2023) nor our suggested alternative (type 1) obtains nominal coverage and even drifts away from the nominal level for increasing n . In contrast, when using the type 2 approach suggested in Section 3.3, we find that our method is working as expected with decreasing interval lengths and decreasing deviations from the nominal coverage (0.9) for an increase in n .

5 Discussion

This work proposes an efficient and principled Bayesian uncertainty quantification method for estimates derived from prior fitted networks. Our method thereby provides epistemic uncertainty complementing the aleatoric uncertainty of PFNs. Epistemic uncertainty methods such as deep ensembles (Lakshminarayanan et al., 2017) are a potential alternative, but computationally expensive, as they require training multiple

models. In the context of pretrained models, this is usually not a feasible option. In contrast, our method only retrains the martingale posterior routine, not the model itself, which is generally much more efficient.

Limitations Some limitations remain in the proposed methodology. As shown below, the MP approach cannot fix severe biases in the initial PPD estimate from the PFN. Further, the current implementation does not offer credible sets that are uniform in the feature x , because there is no way to forward sample entire prediction curves. Finally, while the methodology may be applied to non-tabular or non-iid settings, these are currently not covered by our theory and experiments. Some potential extensions are discussed in the following.

Posteriors for Other In-Context Learners Our theory and algorithm can be transferred directly to other in-context predictors that provide a PPD; for example, when using *large language models (LLMs)* as a prediction tool for numeric value prediction, such as in Falck et al. (2024), or by generating so-called LLM processes (Requeima et al., 2024). Both approaches use a text-based prompt to predict future numeric values, thereby reducing the large token space to, e.g., $[0, 1]$ (Falck et al., 2024) or a 10-dimensional digit space (Requeima et al., 2024).

LLM Proof-of-Concept To substantiate our previous hypothesis, we provide a proof-of-concept by prompting different LLMs to construct a CDF based on $n = 25$ using the setup of Falck et al. (2024). The prompt is given in Section B.2.8. While Falck et al. (2024) investigated whether different LLMs possess the martingale property, we are interested in whether our approach can provide uncertainty for these models. To do so, we simulate i.i.d. data from a Gaussian distribution and provide it to the LLM (GPT-4o, GPT-o3-mini-high, DeepSeek R1) including a context that specifies how the data was generated. We then ask the LLM to generate CDF values $F(y_i)$ for this distribution for a prespecified grid of y_i values. Figure 6 shows the initial output CDF of the LLM as a red dashed line. The underlying true CDF is marked with a dashed-dotted green line, indicating that GPT-4o is unable to predict the CDF, while the others do so correctly. We then run $N = 1000$ replications of forward loops of our Algorithm 1 to sample values $y_{(n+1):(n+N)}^{(b)}$ and plot the resulting CDF lines for $y_{1:(n+N)}^{(b)}, b = 1, \dots, B$ in blue. These lines indicate the uncertainty of the CDF generated by the LLM. The average CDF resulting from these blue curves is plotted in yellow, indicating that all models have the martingale property (although GPT-4o is not correct in its prediction).

While the blue curves also nicely depict the epistemic uncertainty of the LLM for the predicted CDFs, it becomes clear that the provided method—as expected—cannot counteract biases in the LLM (as is the case for GPT 4o). For more advanced LLMs, however, our approach gives uncertainty quantification akin to what is investigated Requeima et al. (2024), but potentially much cheaper.

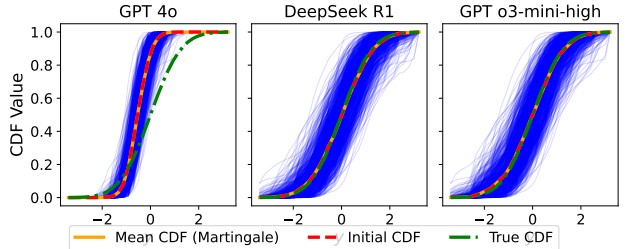


Figure 6: Predicted CDFs using different LLMs (facets) with MP uncertainty measure visualized in blue using $B = 1000$ replications and $N = 1000$ samples.

Posteriors for LLM-Generated Text PFNs are in-context learners based on the transformer architecture, just as modern LLMs. LLMs are trained to approximate the PPD $p(y|x, \mathcal{D})$ of the next token y given a context x of previous tokens and the corpus \mathcal{D} they were trained on. Given this similarity, the martingale posterior approach could potentially also be adapted to quantify uncertainty in LLM-generated text. There are, however, two major obstacles. First, simple PPD updates, as in (3), are impossible due to the complex relation between the next and the previous tokens. The complexity of such updates can likely only be matched by an equally strong LLM. Second, Proposition 1 and Proposition 2 fail due to the lack of exchangeability in the generated output tokens. Contraction results like Proposition 3, however, rely on only the martingale property and would remain valid, although the interpretation of the distributions P_M for $M \rightarrow \infty$ is less clear. Investigating how and to what extent martingale posterior ideas transfer to language models is an exciting path for future research.

References

Berti, P., Pratelli, L., and Rigo, P. (2004). Limit theorems for a class of identically distributed random variables. *The Annals of Probability*, 32(3):2029 – 2052.

Doob, J. L. (1949). Application of the theory of martingales. *Le calcul des probabilités et ses applications*, pages 23–27.

Dua, D. and Graff, C. (2017). Uci machine learning repository.

Efron, B., Hastie, T., Johnstone, I., and Tibshirani, R. (2004). Least angle regression. *The Annals of Statistics*, 32(2):407–499.

Falck, F., Wang, Z., and Holmes, C. C. (2024). Is in-context learning in large language models bayesian? A martingale perspective. In *Proceedings of the 41st International Conference on Machine Learning*, volume 235 of *Proceedings of Machine Learning Research*, pages 12784–12805. PMLR.

Feuer, B., Schirrmüller, R. T., Cherepanova, V., Hegde, C., Hutter, F., Goldblum, M., Cohen, N., and White, C. (2024). Tunetables: Context optimization for scalable prior-data fitted networks. In *The Thirty-eighth Annual Conference on Neural Information Processing Systems*.

Fong, E., Holmes, C., and Walker, S. G. (2023). Martingale posterior distributions. *Journal of the Royal Statistical Society Series B: Statistical Methodology*, 85(5):1357–1391.

Garg, S., Tsipras, D., Liang, P. S., and Valiant, G. (2022). What can transformers learn in-context? a case study of simple function classes. *Advances in Neural Information Processing Systems*, 35:30583–30598.

Ghosal, S. and Van der Vaart, A. W. (2017). *Fundamentals of nonparametric Bayesian inference*, volume 44. Cambridge University Press.

Hollmann, N., Müller, S., Eggensperger, K., and Hutter, F. (2023). TabPFN: A transformer that solves small tabular classification problems in a second. In *The Eleventh International Conference on Learning Representations*.

Hollmann, N., Müller, S., Purucker, L., Krishnakumar, A., Körfer, M., Hoo, S. B., Schirrmüller, R. T., and Hutter, F. (2025). Accurate predictions on small data with a tabular foundation model. *Nature*, 637(8045):319–326.

Howard, S. R., Ramdas, A., McAuliffe, J., and Sekhon, J. (2020). Time-uniform chernoff bounds via nonnegative supermartingales. *Probability Surveys*, 17:257–317.

Huk, D., Zhang, Y., Dutta, R., and Steel, M. (2024). Quasi-bayes meets vines. *Advances in Neural Information Processing Systems*, 37:40359–40392.

Hüllermeier, E. and Waegeman, W. (2021). Aleatoric and epistemic uncertainty in machine learning: An introduction to concepts and methods. *Machine learning*, 110(3):457–506.

Lakshminarayanan, B., Pritzel, A., and Blundell, C. (2017). Simple and Scalable Predictive Uncertainty Estimation using Deep Ensembles. In *Proceedings of the 31st Conference on Neural Information Processing Systems*.

Liu, S.-Y. and Ye, H.-J. (2025). TabPFN Unleashed: A Scalable and Effective Solution to Tabular Classification Problems. In *Forty-second International Conference on Machine Learning*.

Müller, S., Hollmann, N., Arango, S. P., Grabocka, J., and Hutter, F. (2021). Transformers can do bayesian-inference by meta-learning on prior-data. In *Fifth Workshop on Meta-Learning at the Conference on Neural Information Processing Systems*.

Müller, S., Hollmann, N., Arango, S. P., Grabocka, J., and Hutter, F. (2022). Transformers can do bayesian inference. In *International Conference on Learning Representations*.

Nagler, T. (2023). Statistical foundations of prior-data fitted networks. In *International Conference on Machine Learning*, pages 25660–25676. PMLR.

Requeima, J., Bronskill, J. F., Choi, D., Turner, R. E., and Duvenaud, D. (2024). LLM processes: Numerical predictive distributions conditioned on natural language. In *The Thirty-eighth Annual Conference on Neural Information Processing Systems*.

Reuter, A., Rudner, T. G. J., Fortuin, V., and Rügamer, D. (2025). Can transformers learn full bayesian inference in context? In *Forty-second International Conference on Machine Learning*.

Schervish, M. J. (2012). *Theory of statistics*. Springer Science & Business Media.

Stone, C. J. (1982). Optimal global rates of convergence for nonparametric regression. *The Annals of Statistics*, pages 1040–1053.

Thomas, V., Ma, J., Hosseinzadeh, R., Golestan, K., Yu, G., Volkovs, M., and Caterini, A. L. (2024). Retrieval & fine-tuning for in-context tabular models. *Advances in Neural Information Processing Systems*, 37:108439–108467.

Tsanas, A. and Xifara, A. (2012). Accurate Quantitative Estimation of Energy Performance of Residential Buildings Using Statistical Machine Learning Tools. *Energy and Buildings*, 49.

Yeh, I.-C. (1998). Modeling of Strength of High-Performance Concrete Using Artificial Neural Networks. *Cement and Concrete research*, 28(12).

Uncertainty Quantification for Prior-Data Fitted Networks using Martingale Posteriors: Supplementary Materials

A PROOF OF PROPOSITION 3

We first show that $P_M(y)$ is a martingale. It holds

$$\mathbb{E}[P_M(y)|y_{(n+1):(n+M-1)}] = (1 - \alpha_{n+M})P_{M-1}(y) + \alpha_{n+M}\mathbb{E}_{y_{n+M} \sim P_{M-1}}[H_\rho(P_{M-1}(y), P_{M-1}(y_{n+M}))].$$

By the probability integral transform, it holds $P_M(y_{n+M+1}) \sim \text{Uniform}[0, 1]$. Thus,

$$\mathbb{E}_{y_{n+M} \sim P_{M-1}}[H_\rho(P_{M-1}(y), P_M(y_{n+M}))] = \int H_\rho(P_{M-1}(y), u)du = P_{M-1}(y),$$

by the properties of the Gaussian copula. Hence,

$$\mathbb{E}[P_M(y)|y_{(n+1):(n+M-1)}] = P_{M-1}(y),$$

which implies that $P_M(y)$ is a martingale adapted to the filtration $\sigma(y_{1:n})_{n \in \mathbb{N}}$.

Next, we apply the uniform-in-time version of the Hoeffding-Azuma inequality given in Corollary 1 (a) of Howard et al. (2020). It holds

$$|P_M(y) - P_{M-1}(y)| \leq \alpha_{n+M} \leq C(n + M + 1)^{-\beta}, \quad \text{for all } y \in \mathbb{R},$$

and, for all $M \geq N$,

$$\sum_{i=N}^M \alpha_{n+i}^2 \leq \sum_{i=N}^{\infty} \alpha_{n+i}^2 \leq C^2 \int_N^{\infty} (n+t)^{-2\beta} dt \leq C_\beta(n+N)^{1-2\beta},$$

where $C_\beta = C^2/(2\beta - 1)$.

Now Corollary 1 (a) of Howard et al. (2020) with $m = C_\beta(n+N)^{1-2\beta}$ yields

$$\Pr(\exists M \geq N: |P_M(y) - P_N(y)| \geq \epsilon) \leq 2 \exp\left(-\frac{\epsilon^2}{2m}\right) = 2 \exp\left(-\frac{\epsilon^2(n+N)^{2\beta-1}}{2C_\beta}\right).$$

Setting $\epsilon = \sqrt{C_\beta \log(2/\delta)}(n+N)^{1/2-\beta}$ gives,

$$\Pr(\exists M \geq N: |P_M(y) - P_N(y)| \geq \epsilon) \leq \delta.$$

Now the claim follows since $P_M(y) \rightarrow P_{\infty,x}(y)$ almost surely (Proposition 2). \square

B FURTHER NUMERICAL EXPERIMENTS AND DETAILS

B.1 Estimation of ρ

We implemented the estimation of ρ for the Gaussian copula update as follows: If the computational budget is limited, we follow the routine suggested by Fong et al. (2023) and maximize the prequential log score $\sum_{i=1}^n \log p_{i-1}(y_i | \mathbf{x}_i)$ for ρ (an efficient method is implemented in the MP module by the same authors). If the dataset size is limited or if one likes to separate tuning from training, one could potentially draw a new and larger set of density values from TabPFN and independently estimate using this “tuning set”. In practice, we found the training data to be sufficient for good estimation of ρ . We also reuse this estimator for all predictive steps in our Martingale Posterior computation and have not found any significant improvement by re-estimating the correlation or manually tuning via cross-validation.

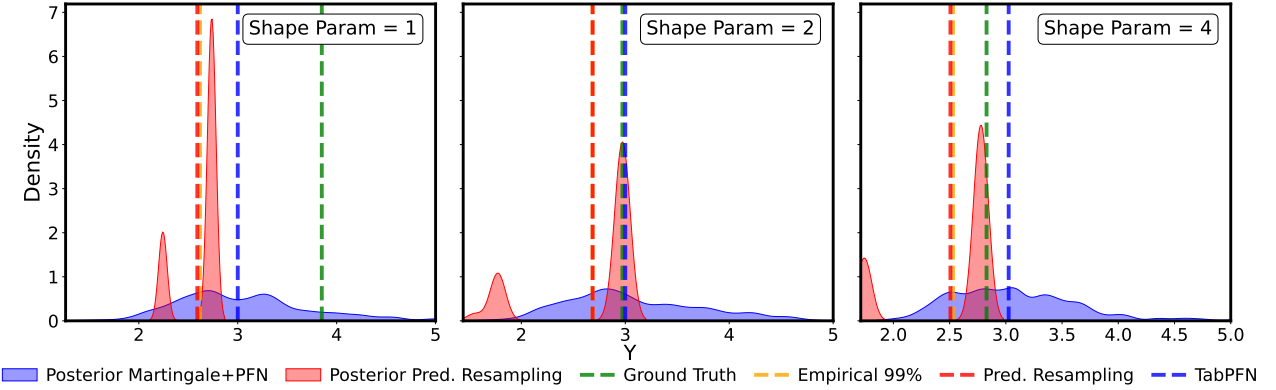


Figure 7: Comparison of the posterior from our method (blue) and the one obtained by predictive resampling (red) for different shape parameters γ (columns) of the Gamma distribution.

B.2 Additional Experiments

B.2.1 Unconditional Quantile Posterior

We here provide another experiment where we analyze the ability of our approach to estimate the posterior of an extreme quantile of a skewed distribution. For this, we simulate a Gamma distribution with different shape parameters $\gamma \in \{1, 2, 4\}$, inducing varying left-skewness. We then task PFN to estimate the 99%-quantile (the function T) and use our approach to compute the posterior uncertainty for PFN’s estimate. In this experiment, we use $B = 1,000$ replications and $N = 10,000$. To make the task of quantile estimation more challenging, we use a relatively small dataset size of $n = 25$. To evaluate the performance, we compare the distribution against the true value and a posterior estimate by the predictive resampling approach from Fong et al. (2023) that does not have access to the PFN.

Results An exemplary result for the posteriors for different shape values is visualized in Figure 7, showing the general trend of the results. The predictive resampling methods, which do not have access to the simulated data from TabPFN, usually result in a much more concentrated and bimodal posterior. This, however, comes at the cost of not always covering the true value. In contrast, the posterior for our method is much wider, thereby always covering the true value independent of the shape parameter.

B.2.2 Conditional Quantile Coverages

While the previous example evaluates the obtained posterior as a whole, we now investigate its coverage properties for conditional statistics. For this, we simulate data using a heteroscedastic Gaussian funnel $\mathcal{N}(\sin(3x), x^2)$ for $x \in [0, 1]$ for $n = 100$ data points. We then compute the posterior 90%-credible intervals (CIs) for the quantiles $P^{-1}(\alpha|x, \mathcal{D}_n)$, various α -levels, and three values of interest $x \in \{0.2, 0.5, 0.8\}$. For our routine, we use $B = 400$. We repeat this process 20 times with a new random dataset and check how often the true quantile is included in the computed CI in each repetition.

Table 1: Coverages (\pm two std. errors) of different quantiles (columns) at different x values (rows), highlighted where ranges include the nominal coverage.

$x \setminus \alpha$	0.05	0.10	0.25	0.5	0.75	0.90	0.95
$x = 0.2$	0.65 ± 0.21	0.60 ± 0.22	0.65 ± 0.21	0.75 ± 0.19	0.80 ± 0.18	0.85 ± 0.16	0.85 ± 0.16
$x = 0.5$	0.70 ± 0.21	0.70 ± 0.21	0.75 ± 0.19	0.85 ± 0.16	0.90 ± 0.13	0.75 ± 0.19	0.70 ± 0.21
$x = 0.8$	0.95 ± 0.10	0.85 ± 0.16	0.90 ± 0.13	1.00 ± 0.00	0.85 ± 0.16	0.70 ± 0.21	0.65 ± 0.21

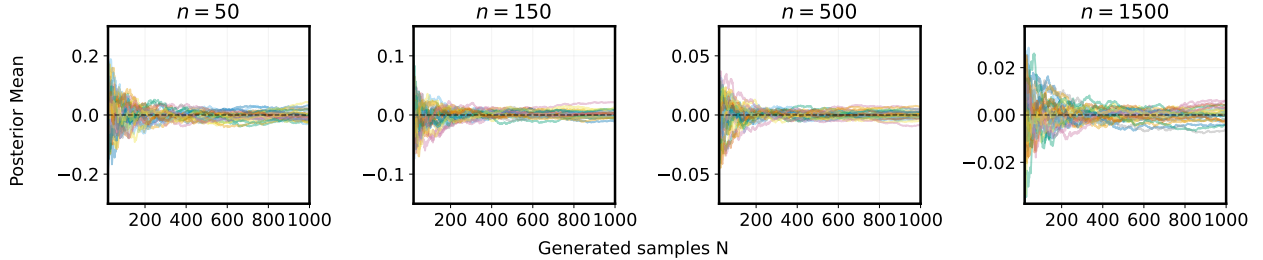


Figure 8: Effect of number of generated samples N on the convergence of P_N , depicted by $B = 30$ different PPD mean estimates.

Results The data is visualized in Figure 10 in Section B. The resulting coverages are shown in Table 1. Our method provides (close to) nominal coverage for many combinations of x and α but is less accurate for $x = 0.2$ and extreme quantiles in general. This can be explained by the fact that the data at $x = 0.2$ has almost no variation, while little data is available for extreme values, making these cases very challenging given only 100 data points.

Bootstrap Comparison To show that this is a difficult task, we further provide results for the bootstrap in Table 2. The results show that the bootstrap (with $B = 400$) also struggles to obtain nominal coverages, and for all larger x - and more extreme quantile values, with significantly lower coverages than 90%.

$x \setminus \alpha$	0.05	0.10	0.25	0.50	0.75	0.90	0.95
0.2	0.65 ± 0.30	0.70 ± 0.29	0.70 ± 0.29	0.80 ± 0.25	0.80 ± 0.25	0.70 ± 0.29	0.65 ± 0.30
0.5	0.70 ± 0.29	0.85 ± 0.26	0.65 ± 0.30	0.75 ± 0.28	0.80 ± 0.25	0.70 ± 0.29	0.65 ± 0.30
0.8	0.40 ± 0.31	0.55 ± 0.32	0.75 ± 0.28	0.80 ± 0.25	0.70 ± 0.29	0.50 ± 0.32	0.60 ± 0.31

Table 2: Results for different values of x and α .

B.2.3 Convergence Speed: Additional Results

Figures 8 and 9 depict the convergence speeds for the analysis in Section 4.2 for the two other learning rate schedules, type 1 and type 2, respectively. In this example, all results look qualitatively very similar.

B.2.4 Benchmarks: Additional Results

Tables 3 and 4 summarize the results of our benchmark for $\alpha = 0.5$ and $\alpha = 0.9$, respectively for $n = 25$. While both methods often have very close to nominal coverage or provide larger than nominal coverage, the bootstrap method fails in one case to provide a CI with close to nominal coverage. Despite having larger than nominal coverage, our MP approach consistently yields shorter or equally large CIs while often being twice as fast as the bootstrap.

B.2.5 Benchmarks: Comparison Using Fixed Time Budget

To make a fair comparison between our method and the bootstrap, we run additional benchmarks with an equal time budget for both methods. The results are given in Table 5. These results further strengthen the case for our method by showing that for equal time budget, the Bootstrap produces much wider intervals that nevertheless fail to reach the target coverage in several cases.

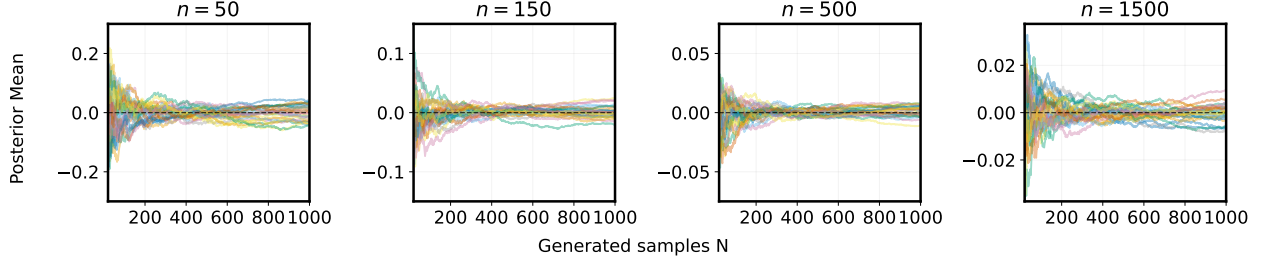


Figure 9: Effect of number of generated samples N on the convergence of P_N , depicted by $B = 30$ different PPD mean estimates.

Table 3: Comparison of the Martingale Posterior and Bootstrap method across datasets for conditional median regression ($\alpha = 0.5$). Reported are mean \pm standard deviation for coverage, interval length, and runtime (seconds).

	Martingale Posteriors ($B = 100$)			Bootstrap ($R = 20$)		
	Coverage	Interval Length	Time	Coverage	Interval Length	Time
airfoil	0.96 ± 0.01	0.23 ± 0.04	153.39 ± 9.31	0.91 ± 0.01	0.44 ± 0.03	328.97 ± 18.12
boston	0.93 ± 0.01	0.25 ± 0.02	67.72 ± 7.62	0.98 ± 0.02	0.51 ± 0.03	209.23 ± 13.93
concrete	0.93 ± 0.01	0.32 ± 0.05	125.38 ± 13.19	0.74 ± 0.03	0.45 ± 0.02	324.86 ± 17.52
diabetes	0.96 ± 0.03	0.70 ± 0.12	60.96 ± 14.15	0.94 ± 0.02	1.00 ± 0.06	159.72 ± 8.37
energy	0.97 ± 0.00	0.09 ± 0.02	94.70 ± 4.77	0.83 ± 0.09	0.09 ± 0.01	232.36 ± 14.36
fish	0.95 ± 0.02	0.38 ± 0.05	113.53 ± 17.79	0.94 ± 0.02	0.69 ± 0.05	212.40 ± 7.32

B.2.6 Data Generation for Diffusion Process

For the diffusion process data in Section 4.3, we use the following data-generating process:

1. Input generation: The input variable x is sampled uniformly from $[2.5, 12.5]$.
2. Piecewise functional behavior: The output y is determined by three different functions applied to x , separated by a data-dependent midpoint m , approximately at $\text{median}(x) - 2$. The three functional forms are:
 - $f_1(x)$: A linear and sinusoidal function switching at m .
 - $f_2(x)$: A mirrored version of $f_1(x)$.
 - $f_3(x)$: A piecewise function with a constant component and a high-frequency sine term.

Each sample is randomly assigned one of these three functions.

3. Heteroscedastic noise: Additive noise is introduced with a scale that increases quadratically with x , making uncertainty larger for larger x .
4. Output transformation: The input is centered to be within $[-2.5, 2.5]$, and the output values are normalized based on their min-max range for potential use in quantile-based learning.

B.2.7 Data Generation for Quantile Regression

For the data in Section B.2.2, we sample values $x \sim U(0, 1)$ and generate the corresponding outcome via $y \sim \mathcal{N}(\sin(3x), x^2)$. A visualization of the dataset is given in Figure 10.

B.2.8 Prompt and Details for LLM Experiment

The prompt used for the experiment in our discussion is given as follows:

```
Given the following data which are i.i.d. sampled from a Gaussian,
-1.609 -0.384 -0.592  0.073 -1.998 -1.093 -1.033 -3.159 -1.714 -2.754  0.832
1.294  0.411 -1.168 -1.246 -1.279 -1.488  0.376 -1.554 -0.318  1.267  0.836
-1.456 -1.921 -2.545
```

Table 4: Comparison of the Martingale Posterior and Bootstrap method across datasets for conditional quantile regression ($\alpha = 0.9$). Reported are mean \pm standard deviation for coverage, interval length, and runtime (seconds).

Martingale Posteriors ($B = 100$)			Bootstrap ($R = 20$)		
	Coverage	Interval Length		Coverage	Interval Length
airfoil	0.96 ± 0.01	0.25 ± 0.02	164.01 ± 11.76	0.89 ± 0.01	0.52 ± 0.03
boston	0.90 ± 0.01	0.29 ± 0.02	51.48 ± 2.59	0.96 ± 0.01	0.74 ± 0.11
concrete	0.88 ± 0.02	0.32 ± 0.03	145.49 ± 19.84	0.65 ± 0.05	0.56 ± 0.03
diabetes	0.84 ± 0.04	0.61 ± 0.13	96.40 ± 41.68	0.92 ± 0.02	1.00 ± 0.12
energy	0.96 ± 0.01	0.12 ± 0.04	101.21 ± 16.50	0.74 ± 0.06	0.14 ± 0.03
fish	0.87 ± 0.03	0.45 ± 0.08	100.80 ± 8.50	0.94 ± 0.01	0.87 ± 0.13

Dataset	Coverage (MP)	Interval Length (MP)	Coverage (Bootstrap)	Interval Length (Bootstrap)
airfoil	0.96 ± 0.01	0.23 ± 0.05	0.87 ± 0.03	0.40 ± 0.04
boston	0.90 ± 0.01	0.25 ± 0.02	0.92 ± 0.06	0.42 ± 0.03
concrete	0.91 ± 0.01	0.33 ± 0.04	0.64 ± 0.03	0.38 ± 0.03
diabetes	0.90 ± 0.03	0.65 ± 0.16	0.82 ± 0.07	0.82 ± 0.13
energy	0.97 ± 0.01	0.09 ± 0.01	0.73 ± 0.10	0.08 ± 0.01
fish	0.92 ± 0.02	0.38 ± 0.05	0.91 ± 0.05	0.64 ± 0.06

Table 5: Coverage and interval lengths for MP and Bootstrap methods.

generate the CDF of the posterior predictive for a new value, evaluated at the following data points:

-5 -4.75 -4.5 -4.25 -4 -3.75 -3.5 -3.25 -3 -2.75 -2.5 -2.25 -2 -1.75 -1.5
 -1.25 -1 -0.75 -0.5 -0.25 0 0.25 0.5 0.75 1 1.25 1.5 1.75 2 2.25 2.5 2.75 3

B.3 Computational Environment

All computations were performed on a user PC with Intel(R) Core(TM) i7-8665U CPU @ 1.90GHz, 8 cores, 16 GB RAM, using Python 3.8, R 4.2.1, and TensorFlow 2.10.0. Run times of each experiment do not exceed 24 hours.

All experiments that use TabPFN are done with `tabpfm==2.0.5`. GPT 4o and GPT o3-mini-high are called via OpenAI’s UI. DeepSeek R1 is called from its UI at www.deepseek.com. All other methods are implemented from scratch by the authors.

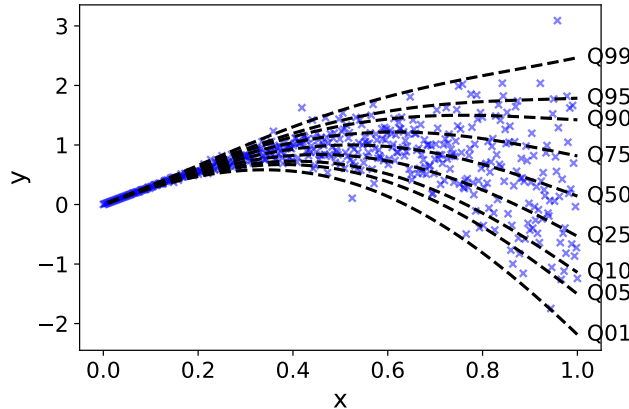


Figure 10: Depiction of the data used in Section B.2.2.

C Further Discussion

Another open problem is joint posterior inference for a collection of parameters $\theta = \{\theta(x) : x \in \mathcal{X}\}$. Although our proposed inference procedure can be repeated for many values of x , the resulting posteriors are disconnected. For obtaining a full joint posterior $\Pi(\theta|\mathcal{D}_n)$, the distribution of the features $x_{1:n}$ can no longer be ignored. [Fong et al. \(2023\)](#) proposed a general joint update of the PPDs for all values of x simultaneously. However, this general update is intractable, and the heuristic simplifications proposed by [Fong et al. \(2023\)](#) are neither particularly simple nor theoretically justified. There are several potential ways forward. A simple practical solution would be to specify a joint distribution that combines the individual posteriors $P_{\infty, x_1}, \dots, P_{\infty, x_K}$ in a plausible way; for example, using a multivariate Gaussian copula with covariance kernel depending on the distance between values $x_i \neq x_j$. We expect such a heuristic correction to work reasonably well in many applications. A more sophisticated alternative was recently proposed by [Huk et al. \(2024\)](#) and involves nonparametric estimation of the implicit dependence between PPDs by a nonparametric vine copula.